Environmental Science & Technology

pubs.acs.org/est

Article

Dissociation of Mercuric Oxides Drives Anomalous Isotope Fractionation during Net Photo-oxidation of Mercury Vapor in Air

Guangyi Sun, Xinbin Feng,* Runsheng Yin, Feiyue Wang, Che-Jen Lin, Kai Li, and Jonas Olof Sommar*

Cite This: *Environ. Sci. Technol.* 2022, 56, 13428−13438

Read Online

ACCESS | Metrics & More | Article Recommendations | Supporting Information

ABSTRACT: The atmosphere is the primary medium for long-distance transport and transformation of elemental mercury (Hg), a potent neurotoxin. The recent discovery of mass-independent fractionation (MIF) of even-mass Hg isotopes (even-MIF, measured as Δ^{200}Hg and Δ^{204}Hg) in the atmosphere is surprising and can potentially serve as a powerful tracer in understanding Hg biogeochemistry. Far-ultraviolet (UVC) light-induced gas-phase reactions have been suspected as a likely cause for even-MIF, yet the mechanism remains unknown. Here, we present the first experimental evidence of large-scale even-MIF caused by UVC-induced (wavelength: 254 nm) Hg oxidation in synthetic air at the pressure (46−88 kPa) and temperature (233−298 K) resembling those of the lower atmosphere. We observe negatively correlated Δ^{200}Hg and Δ^{204}Hg signatures with values as low as −50‰ and as high as 550‰, respectively, in the remaining atomic Hg pool. The magnitude of even-MIF signatures decreases with decreasing pressure with the Δ^{200}Hg/Δ^{204}Hg ratio being similar to that observed in global precipitation. This even-MIF can be explained by photodissociation of mercuric oxides that are photochemically formed in the UVC-irradiated Hg−O_2 system. We propose that similar processes occurring in the atmosphere, where mercuric oxide species serve as intermediates, are responsible for the observed even-MIF in the environment.

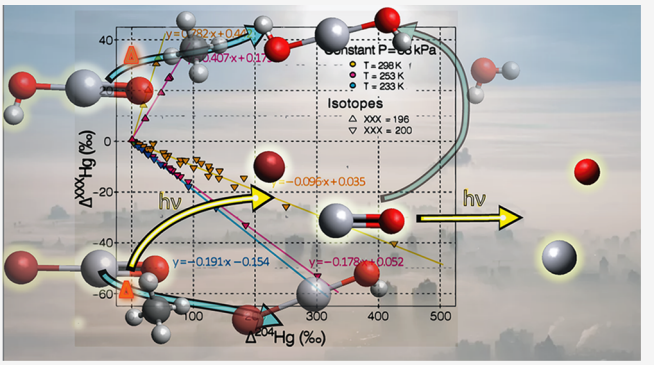

KEYWORDS: *mercury, stable isotope fractionation, mass-independent fractionation, photochemistry, atmosphere*

INTRODUCTION

Mercury (Hg) is among the top 10 chemicals of public health concern by the World Health Organization, due to its high volatility to transport in the atmosphere, active redox chemistry, strong accumulation in food webs, and potential toxicity to human and ecosystem health. Anthropogenic emissions of Hg to the environment are regulated under the United Nations Minamata Convention. The complex atmospheric cycling of Hg is fundamental for its dispersion into global ecosystems, but key processes such as oxidation and reduction in the atmosphere remain inadequately characterized.[1] One of the most promising new tools that may help understand these processes is Hg isotopes. Hg isotopes undergo both mass-dependent fractionation (MDF; measured typically as δ^{202}Hg) and mass-independent fractionation (MIF). MIF of odd isotopes (odd-MIF, measured typically as Δ^{199}Hg and Δ^{201}Hg) has been observed in a number of processes (e.g., Hg^{II} photoreduction, MeHg photodegradation processes, and Hg(0) evaporation) and explained by magnetic isotope effect (MIE)[2] or nuclear volume effect (NVE).[3] MIF of even isotopes (even-MIF,[4] measured typically as Δ^{200}Hg and Δ^{204}Hg) so far has been observed only in samples that are of the atmospheric origin or have been influenced by atmospheric deposition.[5] However, neither MIE nor NVE can explain this type of MIF to any substantial degree. An atmospheric budget indicates significant imbalances between Δ^{200}Hg in Hg emissions from and deposition to the Earth's surface, which, to be in a steady state, require atmospheric even-MIF sources.[6] A reaction mechanism proposed to trigger even-MIF has been associated with Hg photo-oxidation in the troposphere or in the upper atmosphere.[7] In support, it has been claimed that Δ^{200}Hg/Δ^{204}Hg ratios observed in nature have some similarity to those occurring in the glass housing of compact fluorescent lamps (CFLs),[8,9] but in fact $\Delta^{199}Hg^{II}$, $\Delta^{200}Hg^{II}$, and $\Delta^{204}Hg^{II}$ in the CFL housing bear opposite signs to what is observed in nature.[6] Recently, rock records have shown significant even-MIF in the Archean atmosphere lacking an ozone (O_3) layer to filter UVC from actinic light, suggesting that contemporary UVC-induced atmospheric chemistry could be responsible for the coupled changes in both even-Hg-MIF and sulfur-MIF.[10]

Received: April 20, 2022
Revised: August 1, 2022
Accepted: August 1, 2022
Published: August 12, 2022

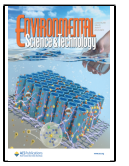

Despite being a prevailing hypothesis, so far there has been no convincing evidence, either theoretically or experimentally, to support the importance of even-MIF during atmospheric Hg photo-oxidation nor the underlying mechanism. Previously, we have experimentally investigated the oxidation of atmospheric gaseous Hg by Cl and Br atoms, yielding product vapors that condense under laboratory conditions (ppb-level) and could be scanned as nanometer-sized particles.[11] The atomic Cl-initiated reaction generates a low but significant even-MIF, while the Br-initiated reaction gives a negligible even-MIF. Although the reaction is fast, the Cl-initiated oxidation is not considered important due to the very low Cl background concentration in the troposphere ($\leq 10^3$ atoms cm^{-3}).[12] The Br study has a deficient Δ^{200}Hg isotope mass balance making it impracticable to determine conclusively whether even-MIF is present.[11] Recently, Fu et al.[6] have interpreted our experimental results such that limited even-MIF is the result of heterogeneous redox chemistry driven by suspended nanoparticles emanating from the products of the pure gas-phase Hg oxidation. They suggested that hyperfine coupling between the spins of magnetic halogen atoms (e.g., ^{35,37}Cl and ^{79,81}Br) and unpaired electrons of even-Hg isotopes was the cause of even-MIF. Their interpretation is tentative, as is their stoichiometrically unbalanced reaction scheme.[6] Reporting of all seven Hg stable isotopes as tracers is desirable in the interpretation of process-oriented studies, and unfortunately, analyses of the lightest (^{196}Hg) and heaviest (^{204}Hg) of them are missing in many laboratory and field studies.[6]

In this study, we focus on reactions of the Hg−O_2 system that exhibits intricate complexity. A direct combination of liquid Hg and O_2 occurs just below the boiling point of Hg (357 °C at 101 kPa) to form HgO, but the reaction is reversed above 400 °C.[13] The reaction of ground-state singlet Hg atoms ($Hg(^1S)$) with O_2 is very slow (rate $\leq 10^{-23}$ cm^3 $molecule^{-1}$ s^{-1}) in the gas phase and has no significance in the atmosphere.[13] In contrast, upon light excitation of $Hg(^1S)$, the formed triplet Hg atoms ($Hg(^3P)$) react rapidly with O_2.[14] This UVC-induced reaction that involves the formation of O_3 is not clearly understood and competitive exit channels are in operation during the quenching process. Energy transfer from $Hg(^3P)$ atoms generates vibrational hot ground-state O_2[15]

$$Hg(^3P) + O_2 \rightarrow Hg(^1S) + O_2^* \quad \text{(R1)}$$

The activated oxygen (O_2^*) produced may react by[16]

$$O_2^* + O_2 \rightarrow O_3 + O(^3P) \quad \text{(R2)}$$

which is followed by[16]

$$O_2 + O(^3P) \xrightarrow{M} O_3 \quad \text{(R3)}$$

where M represents a third body (e.g., N_2, O_2). Simultaneously, Hg vapor is consumed with the product HgO observed as yellow-brown stains on reactor walls.[17] However, the mechanism is unelaborated, there is debate regarding the molecular intermediates, and whether the reactant starting the oxidation is a $Hg(^3P)$ or a $Hg(^1S)$ state remains a subject of dispute.[15] However, gas-phase oxidation of $Hg(^1S)$ directly to HgO by O_3 is not feasible because the O atom transfer step is highly endothermic,[18] which limits the number of possible exit channels[19]

$$Hg(^3P) + O_2 \rightleftarrows HgO_2^* \quad \text{(R4)}$$

$$HgO_2^* \overset{M}{\leftrightarrow} HgO_2 \quad \text{(R5)}$$

$$HgO_2 \rightarrow HgO + O(^3P) \quad \text{(R6)}$$

$$HgO_2 + O_2 \rightarrow HgO + O_3 \quad \text{(R7)}$$

where HgO_2^* represents an activated complex. It has been shown that it is not the short-lived $Hg(^3P_1)$ but rather the spin−orbit relaxed and radiatively metastable $Hg(^3P_0)$ state that drives R4.[19] The two main constituents of air play different roles in the process, with N_2 deactivating $Hg(^3P_1)$ almost exclusively to $Hg(^3P_0)$, while O_2 quenches both $Hg(^3P_1)$ and $Hg(^3P_0)$ directly to $Hg(^1S)$ (cf. R1).[14] Thus, the production of HgO_2 (R4) benefits from air rather than O_2 alone.

We hypothesize that the reactions initiated by $Hg(^3P)$ in air are responsible for even-MIF since they lead to large-scale isotope enrichment[20] due to their high rate and exothermic characteristics.[14] The oxidant, O_2, is a major constituent of the atmosphere. However, direct spectroscopic measurement of the $Hg(^3P) + O_2$ system is challenging due to the trapping of resonance radiation $Hg(^1S) + h\nu \rightarrow Hg(^3P)$[15] where the lifetime of $Hg(^3P)$ depends on both the Hg concentration and the pressure of the bath gas. Moreover, O_3 absorbs UV strongly ($\sigma = 1.17 \times 10^{-17}$ cm^2) and is photolyzed ($O_3 + h\nu \rightarrow O(^1D) + O_2^*$) at the excitation wavelength (253.7 nm) of the transition $Hg(^1S_0) \rightarrow Hg(^3P_1)$.[16] In contrast to previous studies (ppm-level), we perform the photolysis study with such low Hg concentrations (ppb-level) that combined kinetic and isotope changes can be observed closer to typical atmospheric conditions without radiation trapping. We also use a Zeeman system[21] to individually detect atomic Hg in the presence of optically interfering species such as O_3. Further details of the experimental setup can be found in the Materials and Methods section.

MATERIALS AND METHODS

Photolysis Experiments. The experiments were carried out in FEP Teflon-film chambers described previously in Sun et al.[11] (Figure S1), which also accounts for the reactant preparation, at different temperatures (233, 253, and 298 K) and pressures (88, 61, and 46 kPa) with UVC light supplied from Hg low-pressure lamps (TUV G5 4W, Phillips) (Figure S2). Hg-containing dry synthetic air (mixing ratio ranging from 0.7 to 3.5 parts-per-billion (ppb)) was irradiated for up to 300 min to allow for the oxidation to proceed over a range of the remaining Hg fraction (f_R). The low-pressure lamps containing a natural mixture of Hg isotopes (Table S1) were illuminating essentially at 254 nm (∼5 nm full width at half maximum measured by a spectroradiometer, Figure S2) but filtering out 185 nm O_3-forming UVC radiation. The experiments were carried out with a light flux of $\sim 1.4 \times 10^{13}$ photons cm^{-2} s^{-1} and an optical thickness of <0.1. Decays of Hg were monitored by a portable Zeeman modulated atomic absorption spectrometer (Z-AAS, Model RM-915+, Lumex Instruments), and f_R at the end of experiments was systematically varied over the range $1 > f_R > 0.2$ by the duration of photolysis time. After an experiment reached the stipulated f_R, the reaction mixture was evacuated from the chamber into a wet chemical Hg speciation sampling train described in detail by Sun et al.[11] O_3 in the reaction mixture was determined in a differential way by simultaneous monitoring by a Thermo 49i instrument (detecting both O_3

https://doi.org/10.1021/acs.est.2c02722
Environ. Sci. Technol. 2022, 56, 13428−13438

and Hg) and the Z-AAS instrument mentioned above (detecting only Hg). Consequently, accurate calibrations of the Model 49i instrument's response to both O_3 and Hg were performed continuously. In experiments involving the measurement of Hg isotopic ratios, Hg vapor was generated from reduction of a NIST-3133 Hg standard solution (in ~0.1 M HCl) by adding excess $SnCl_2$ followed by purging using a Hg-free zero air stream into the reaction chamber. For reference, the slow light-independent gas-phase reaction between Hg and O_3 with respect to isotope fractionation was studied (Table S5). We have also checked that the loss of gaseous Hg in air is negligible in UVB (290−315 nm) light as expected.[13]

Isotope Composition Measurements and Data Evaluation. Hg isotopic ratios for all samples were determined by a Nu-Plasma II cold-vapor multicollector inductively coupled plasma mass spectrometer (Nu Instruments Ltd., U.K.). The sample introduction system consists of a continuous flow cold-vapor generation system (CV) (HGX-200, CETAC) coupled to an Apex-Q desolvation unit (Elemental Scientific Inc.) for Hg and Tl introduction, respectively. $SnCl_2$ is used as the reducing agent and mixed online with Hg standards or samples to generate volatile Hg. Hg vapor from the CV generation system is mixed with a dry Tl aerosol produced via the desolvation device. Instrumental mass bias correction was achieved using Tl (NIST SRM 997) as an internal standard and external standard-sample bracketing with a NIST SRM 3133 Hg solution. A typical sequence includes measuring the NIST-3133 Hg standard before and after each sample. The acid and Hg concentrations of the bracketing solution were systematically adjusted to within 10% of the sample. On-peak-zero mode was used during all measurements. MDF is reported in the δ-notation

$$\delta^{xxx}\mathrm{Hg} = \left\{ \frac{(^{xxx}\mathrm{Hg}/^{198}\mathrm{Hg})_{\mathrm{sample}}}{(^{xxx}\mathrm{Hg}/^{198}\mathrm{Hg})_{\mathrm{NIST3133}}} - 1 \right\} \times 10^3 (‰) \quad (1)$$

where ^{xxx}Hg is each isotope between 196 and 204. MIF is reported in Δ-notations, which are following Bergquist and Blum[22] calculated by

$$\Delta\mathrm{Hg}^{xxx} = 1000 \cdot (\{\ln[(\delta^{xxx}\mathrm{Hg}/1000) + 1]\} - \beta_{xxx} \cdot \{\ln[(\delta^{202}\mathrm{Hg}/1000)] + 1\}) \quad (2)$$

where

$$\beta_{xxx} = \ln(m_{198}/m_{xxx})/\ln(m_{198}/m_{202}) \quad (3)$$

and m_{xxx} is the atomic mass of the Hg isotope of interest and β_{xxx} values for xxx = 196, 199, 200, 201, and 204 are −0.508, 0.252, 0.502, 0.752, and 1.493, respectively.

The kinetic fractionation factors (α) of Hg during the processes can be estimated as Rayleigh distillation describing a sink of pseudo-first kinetic order in a closed system

$$R^{xxx/198} = R_0^{xxx/198} \cdot f_R^{(\alpha^{xxx/198} - 1)} \quad (4)$$

where R and R_0 are ^{xxx}Hg/^{198}Hg ratios for the residual and initial product, respectively, and α is the ratio of the heavy-to-light isotope oxidation rates. Introducing the δ-notation, eq 4 can be approximated by

$$\ln \frac{1000 + \delta^{xxx}\mathrm{Hg}}{1000 + (\delta^{xxx}\mathrm{Hg})_0} = (\alpha^{xxx/198} - 1) \cdot \ln(f_R) \quad (5)$$

where $(\delta^{xxx}\mathrm{Hg})_0$ is the initial δ^{xxx}Hg value of the reactant and the slope represents $\alpha^{xxx/198} - 1$ (unit ‰). Full details about the isotope composition of samples used in this study are provided in the SI, Materials and Methods section. The long-term reproducibility of the isotope measurements was assessed by repeated measurements of NIST 3177 ($HgCl_2$) standard solutions (Table S2).

RESULTS

Kinetics and Product Formation. The photo-oxidation rate coefficient J (s^{-1}) of Hg in air is given by

$$J = -\ln(f_R)/t \quad (6)$$

where f_R represents the proportion of Hg remaining in the reaction mixture after time t in relation to the initial value at t = 0 ($f_R = [\mathrm{Hg}]_t/[\mathrm{Hg}]_0$). Under 253.7 nm irradiation, the concentration of Hg in air experienced the first-order decrease over time at the pressure range of 46−88 kPa and temperature range of 233−298 K. Since the termination of irradiation discontinues further Hg loss, we conclude that it is the excited state ($Hg(^3P)$) and not ground-state ($Hg(^1S)$) atoms that drive the oxidation over the examined time scale. The J value is calculated for each of the investigated pressures and temperatures by plotting the natural logarithm of [Hg] vs irradiation time (Figure 1). The slopes of the linear fit (representing J) fall

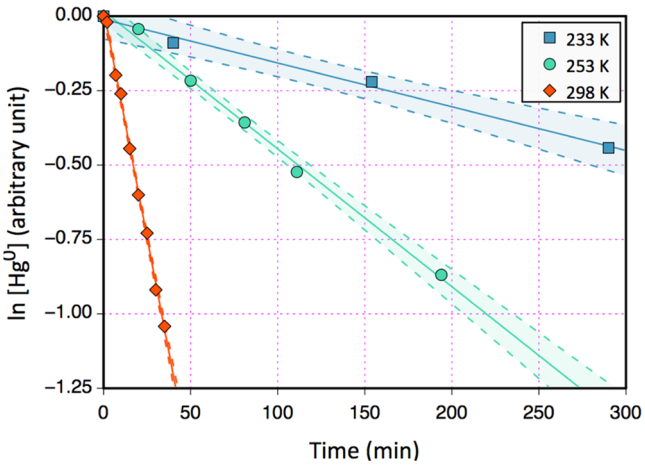

Figure 1. First-order plots of loss of Hg at 88 kPa over time at different temperatures. The envelope within the dashed lines represents the 95% confidence interval.

in the range from 2.5×10^{-5} to 1.0×10^{-3} s^{-1} (Table S3). In turn, the pressure- and temperature-dependent J is proportional to the Hg absorption cross-section ($\sigma = 2.5 \times 10^{-14}$ cm^2 at unity atmospheric pressure[23]), the quantum yield for Hg oxidation (ϕ), and the photon flux (photons cm^{-2} s^{-1}) at λ = 253.7 nm. Given a photon flux of 1.4×10^{13} cm^{-2} s^{-1}, the calculated ϕ for the oxidation channel (R4) is small at all pressures and temperatures (≤0.03, Table S3). The pressure dependence of J suggests a chemically activated reaction type (R4−R6).[24] Consequently, behind an observational net recombination of Hg (^{3}P) and O_2 plausibly hides a complex chemical system with elements of reversible redox reactions (SI, Section 1).

The temperature dependence of J is fitted by the exponential Arrhenius equation when ln J was plotted vs T^{-1} (Figure 2A). The corresponding activation energy was determined to be

https://doi.org/10.1021/acs.est.2c02722
Environ. Sci. Technol. 2022, 56, 13428−13438

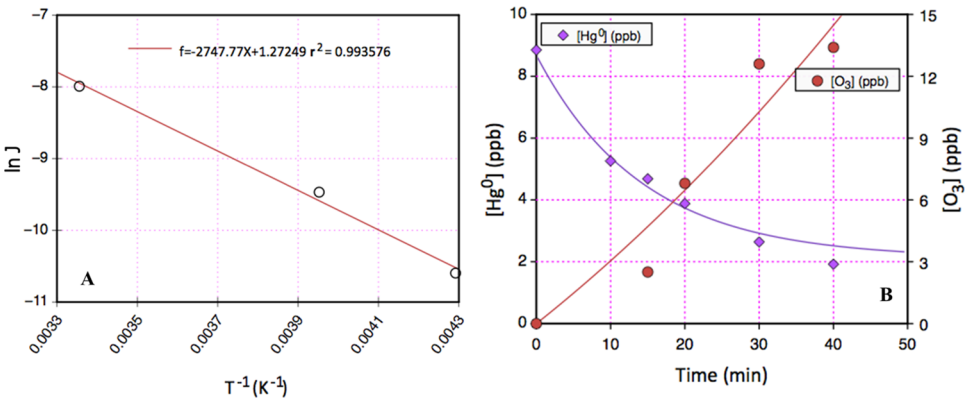

Figure 2. (Left) Plot of ln J (s^{-1}) versus inverse temperature T (K^{-1}). The slope of the fitted line corresponds to an activation energy of 22.8 kJ mol^{-1}. (Right) Progression of Hg loss and O_3 formation with irradiation time in the reaction mixture during a typical experiment at 298 K and 88 kPa.

22.8 ± 4.6 kJ mol^{-1}, which is small compared to that of the Hg(^{3}P) state (~249 kJ mol^{-1} [25]). As shown in Figure 2B, the loss of Hg in the synthetic air was accompanied by the formation of O_3. Previous studies on the Hg(^{3}P) + O_2 system, conducted at higher Hg concentrations, higher temperatures, and higher photon fluxes,[17,19,26] claimed that from 7[17] up to 60[26] molecules of O_3 were formed per atom of lost Hg. In this study, we observe significantly lower ozone yields at 298 K, around 2 to 3 molecules of O_3 per atom of Hg lost. The lower yields can be explained by competing reactions. Reaction 6 followed by R3 and reaction 7 produce one ozone molecule per lost Hg atom. Another series involves Hg merely as a photosensitizer via R1, which is then followed by R2 and R3.

Isotope Fractionation in Residual Hg during the UVC-Induced Oxidation. The Hg isotopic results from the experiments are given in Table S4, which shows both experimental parameters and the isotope composition of the remaining Hg in the reaction mixture (f_R, eq 4) for each run. The mass dependence was evaluated using the kinetic mass-dependent fractionation law,[27] and Figure S3 shows least-squares fits to Rayleigh plots for the 88 kPa study (eq 5) at 298, 253, and 233 K, where kinetic fractionation factors $\alpha^{202/198}$ are calculated from the slopes to be −12.0 ± 0.8, 74.2 ± 28.1, and 57.7 ± 13.1‰, respectively. However, all of these values exceed the limit of ~10‰, which is theoretically possible by kinetic and equilibrium MDF combined. Therefore, the arbitrarily chosen mass-dependent fractionation based on the ratio between 202 and 198 is likely biased as these even-numbered isotopes in themselves are also fractionated in a mass-independent manner. By comprehensively measuring all stable Hg isotopes including the five with even mass numbers, we may construct alternative systematics using an odd−even standard (e.g., ^{199}Hg/^{198}Hg) instead of ^{202}Hg/^{198}Hg in the definition of δ^{xxx}Hg.[28] The recalculated result highlights the behavior of ^{202}Hg alongside ^{196}Hg, ^{200}Hg, and ^{204}Hg. Figure 3 clearly shows that under the pressure and temperature conditions examined, all of these Hg even isotopes are fractionated in an anomalous mass-independent manner during the oxidation process. The observation of coherent linear trends between the arrays of $\Delta^{196/198}$Hg, $\Delta^{200/198}$Hg, $\Delta^{202/198}$Hg, and $\Delta^{204/198}$Hg further strengthens our interpretation of a mechanism that does not comply with conventional MDF calculated by $\alpha^{xxx/198} = (\alpha^{202/198})^{\beta xxx}$ (for β^{xxx}, see eq 3). The reaction between ground-state Hg and ozone as a potential source of secondary Hg oxidation in the Hg + O_2 system, on the other hand, follows low-level MDF (Figure S4 and Table S5) and cannot give rise to the strong MIF overprint in the reaction mixture. This follows that MDF as described by the kinetic isotope theory applies to isotope effects arising from the rate-limiting step of thermally driven processes. For the heaviest elements such as Hg, NVE also contributes to determining net MDF[3].

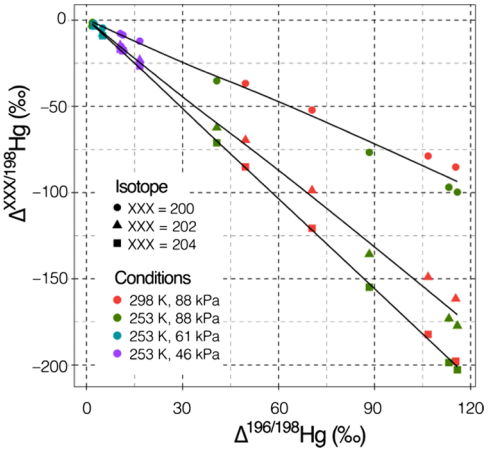

Figure 3. Relationship between MIF for the array of even-Hg isotopes using an alternative odd/even isotope ratio standard.

Returning to reporting Hg isotope fractionation as recommended by Bergquist and Blum, the result of the evaluation of the multi-isotope MIF is shown in Figures 4 and 5. The magnitude of MIF decreases in the order ^{204}Hg > ^{199}Hg ~^{196}Hg > ^{201}Hg > ^{200}Hg and the overall magnitude tends to increase with temperature and pressure. These physical dependencies are evidence that the origin of MIF stems from the dissociation of labile mercury oxides (back reactions, see discussion below). Odd-MIF signatures (Δ^{199}Hg and Δ^{201}Hg) have the same sign (positive in the Hg^0 pool) while its ratio Δ^{199}Hg/Δ^{201}Hg attains an increasing slope with increasing temperature (1.43, 1.44, and 1.87 at 233, 253, and 298 K, respectively, Figure 4, left) at 88 kPa. Odd-MIF ratios reported for CFL-trapped Hg[8] show a substantial scatter falling in the range of −1.9 to −1.1 and for Δ^{199}Hg consistently carry a negative sign (Figure 4, right). Again for even isotopes, CFL-trapped Hg data show a diffuse distribution with weak correlations between Δ^{196}Hg, Δ^{200}Hg, and Δ^{204}Hg (Figure 5 right). In our study, Δ^{200}Hg and Δ^{204}Hg show values with

https://doi.org/10.1021/acs.est.2c02722
Environ. Sci. Technol. 2022, 56, 13428−13438

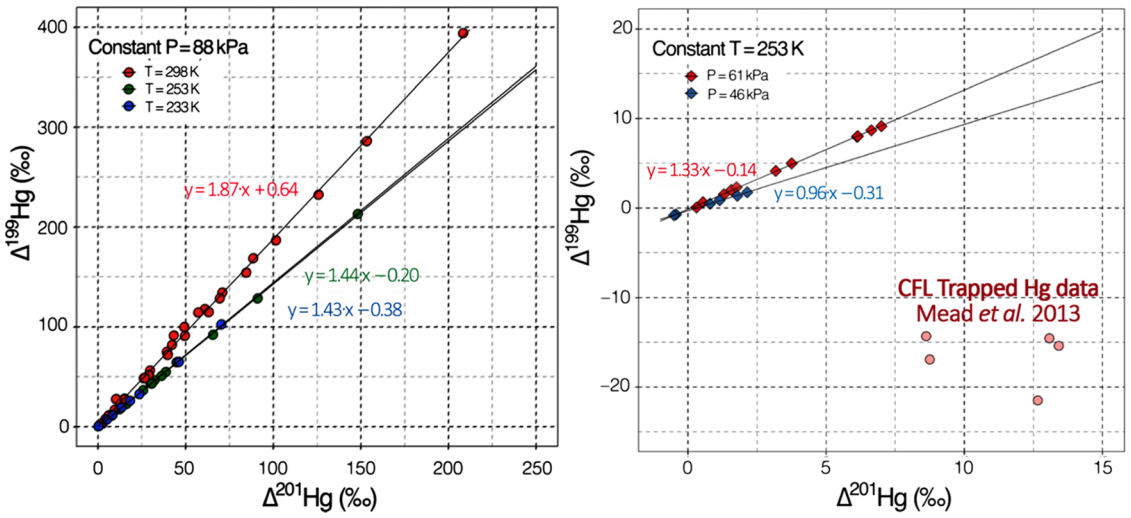

Figure 4. Scatterplots of Δ^{199}Hg vs Δ^{201}Hg trajectories in the remaining Hg during photo-oxidation at a constant pressure (88 kPa) but different temperatures (left) and at a constant temperature (253 K) but different pressures of 46 and 61 kPa (right). Literature data on trapped (oxidized) Hg in the glass frame of CFL has been entered in the right figure (filled circles).

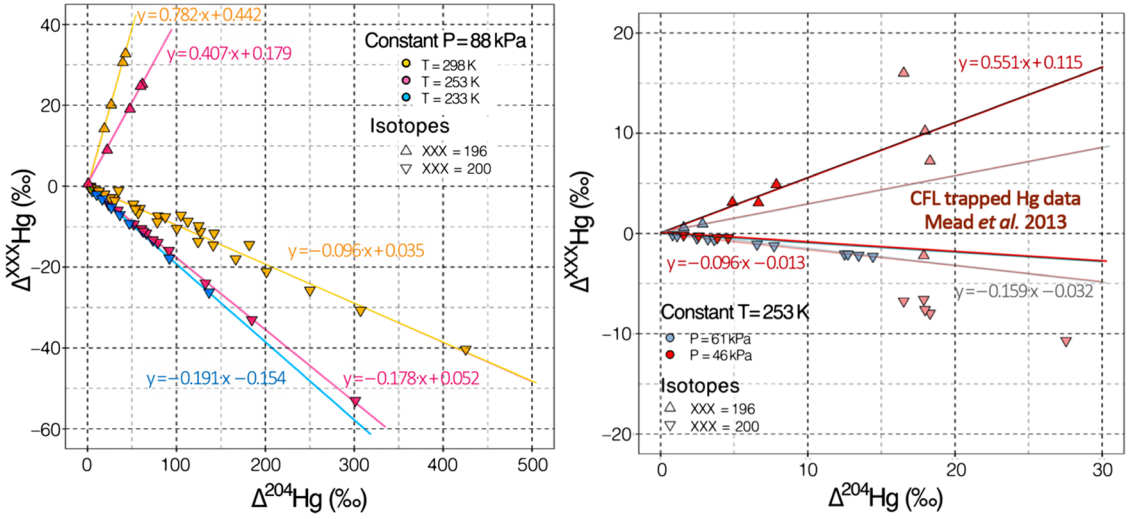

Figure 5. Scatterplots of Δ^{200}Hg vs Δ^{204}Hg trajectories in the remaining Hg during photo-oxidation at the three investigated temperatures of isobaric conditions at 88 kPa (left). At the two higher temperatures, the left panel is supplemented with Δ^{196}Hg−Δ^{204}Hg data. In the right panel, the Δ^{196}Hg and Δ^{200}Hg scatter versus Δ^{204}Hg are reported under isothermal conditions (253 K) at the two reduced pressures of 46 and 61 kPa. Literature data on trapped (oxidized) Hg in the glass frame of CFL has been entered in the right figure (rosy brown filled markers toward the right) as well. The latter dataset contains one Δ^{196}Hg−Δ^{204}Hg value that is outside the scale in right.

opposite signs, and the even-MIF diagnostic ratio (Δ^{200}Hg/Δ^{204}Hg) increases at 88 kPa from −0.19 at 233 to −0.09 at 298 K (Figure 5 left). In the same panel, we also show in the left panel of Figure 5 correlations of Δ^{196}Hg with Δ^{204}Hg (ratios of 0.78 and 0.41 at 298 and 253 K, respectively, at 88 kPa). Considering the low-temperature and low-pressure conditions resembling high altitudes, the Hg isotope fractionation at lower pressures (46 and 61 kPa) at 253 K is also investigated. As shown in Figure 4, the Δ^{199}Hg/Δ^{201}Hg ratio decreases with decreasing pressure, from 1.44 at 88 kPa to 1.33 at 61 kPa and 0.96 at 46 kPa. Consequently, the low pressure and temperature suppress the magnitude of Δ^{199}Hg/Δ^{201}Hg. In contrast, the Δ^{200}Hg/Δ^{204}Hg ratio increases slightly at 253 K with decreasing pressure, from −0.18 at 88 kPa to −0.16 at 61 kPa and −0.10 at 46 kPa. As shown in Figure 5, right, the Δ^{200}Hg/Δ^{204}Hg ratio thus appears to attain a shallow minimum value at reduced atmospheric pressure and freezing temperatures (253 and 233 K).

Gaseous Hg^0, the major form of Hg in the atmosphere,[29] is oxidized to gaseous Hg^{II} species,[30] which are water-soluble, partition to particulates,[31] and thus easily scavenged by precipitation. A regression analysis based on pooled global precipitation samples shows a Δ^{200}Hg/Δ^{204}Hg slope of −0.2,[5] which is consistent with our experimental data. Considering that the relationship between Δ^{200}Hg and Δ^{204}Hg shows large spatial and temporal scattering in global samples (Figure S5), the photoredox chemistry presented in this work can partially explain even-MIF in the atmospheric environment, where mercury exhibits complex redox chemistry not only in clouds and aerosols but also in the gas phase on a shorter time scale in parallel with physical removal. Rapid gas-phase photoreduction of major Hg^{II} species produced in the atmosphere takes place leading to gaseous Hg^0 being indirectly or directly regenerated

https://doi.org/10.1021/acs.est.2c02722
Environ. Sci. Technol. 2022, 56, 13428−13438

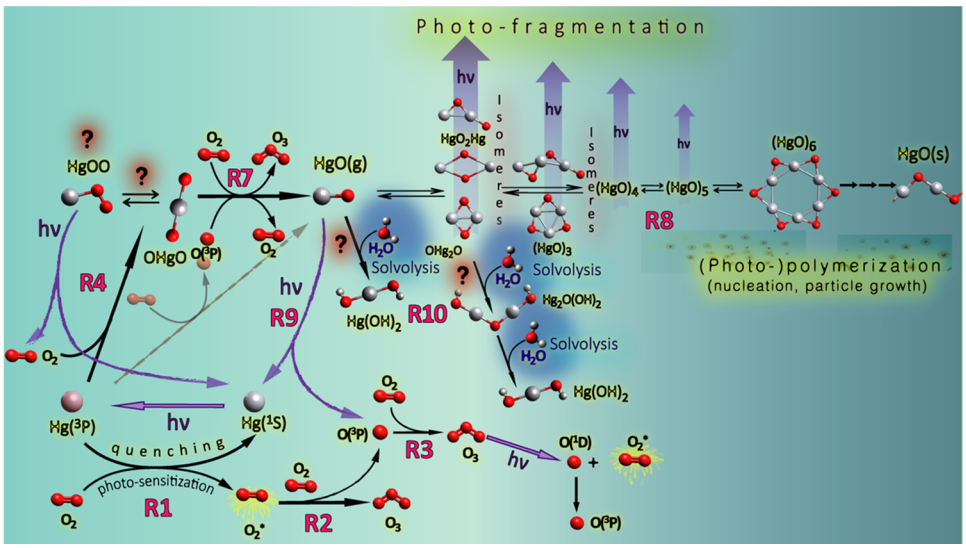

Figure 6. Summary of proposed reactions occurring in the Hg−O_2 system with 254 nm light present. Secondary chemistry involving H_2O to potentially stabilize the HgO_x reaction products by solvolysis in the atmosphere has been included.

as suggested by Saiz-Lopes et al.[1] As described below, we attempted to derive the origin of MIF from photoreductive processes in the UVC light chemically activated Hg + O_2 system. Since similar unimolecular dissociative processes are central to the atmospheric cycling of mercury, our results may indicate that even-MIF triggering is characteristic of multiple gas-phase Hg^{II} photolysis reactions.

Reaction Mechanisms and Origin of the Anomalous Isotope Effect. Although the values of the $\Delta^{199}Hg/\Delta^{201}Hg$ ratio observed in this study (ranging from 1.0 to 1.9) may indicate controls from either MIE or NVE, the magnitude of the odd-MIF is different from what was previously reported for processes studied in the laboratory and the field. MIE is imparted by a radical pair mechanism linked to the restricted movement of radicals relative to one another (cage effect), which occurs in the gas phase only at high pressures.[32] NVE has been described for equilibrium exchange reactions but has never been expanded to kinetic processes. Deviating from the low magnitude observed in natural samples, the possibility that nonequilibrium isotope effects of NVE in photodissociation may give rise to a significant magnitude of MIF has recently been suggested.[33] Nevertheless, for equilibrium fractionation, NVE-driven even-MIF is minor in relation to odd-MIF and is also of the opposite sign to $\Delta^{200}Hg$ signals observed in nature.[34] Prior to this study, large MIF of even-Hg isotopes was observed only inside CFL,[8] where the MIF is confined to a very small fraction (≪1% of the total Hg in the CFL) of mixed oxidation states that gives a dark coloration.[35] This small Hg fraction is incorporated into the glass probably by diffusion of Hg ions generated in the plasma.[35] Sulfur- and oxygen-MIF has been documented in a number of gas-phase reactions with several hypotheses proposed for the underlying mechanism(s). They include symmetry-, abundance-, and reaction rate-dependent isotope selective mechanisms.[36] The observation of enrichment of all Hg isotopes relative to the most common one (^{202}Hg) in a CFL led Mead et al. to suggest the presence of an abundance ratio-dependent effect.[8] The conditions for one of these, self-shielding, are favorable during radiation trapping but cannot satisfactorily explain the MIF observed in CFL.[8]

It is important to recognize the differences in operating conditions in a CFL from those in the reaction chamber used in the present study. A CFL atmosphere is characterized by low pressure (400 Pa), the presence of an inert filling gas (Ar), and a typical Hg vapor−liquid equilibrium temperature of 40−60 °C.[37] Most of the input power of Hg−Ar discharges in CFL (standard Hg mixing ratio > 1000 ppm) is released as 254 nm light. Because of radiation trapping, the effective lifetime of $Hg(^3P_1)$ in a CFL is much longer than that in our study. In addition to the divergent $Hg(^3P_1)$ lifetimes, the isotopic and hyperfine components of the 254 nm Hg line appear as five fully resolvable groups in a standard CFL atmosphere[38] but as a single, broad absorption profile at the pressure range of our experiment.[23] Self-shielding should not be important in our experiment since the effect benefits from the Hg absorption features do not overlap,[36] as is the case in a CFL but not in our experiment. Precipitation analysis of all stable Hg isotopes distribution now implies that self-shielding lacks relevance in the atmospheric chemistry of Hg.[6] Isotope-dependent kinetic differences are not expected in our photolysis experiments concerning the $Hg(^3P)$ chemistry[39] but could be the case for the photochemistry of the oxidized Hg pool.

The observed MIF increase with pressure and temperature together with kinetic data indicates that dissociative processes rather than recombination within the framework of chemically activated reactions can be sources of the anomalous isotope effect. A combination between $Hg(^3P)$ and O_2 yields isotope-enriched HgO if the light source containing an excess of the target Hg isotope and a scavenger (e.g., a diene) is added to the air mixture.[20] Such photochemical isotope separation proceeds under conditions promoting radiation trapping.[20] Using relatively low Hg concentration and atmospheric pressure, Hippler et al.[15] observed formation of a long-lived excited intermediate that was in a previous study[40] assigned to HgO_2 tentatively produced by R4 + R5. The overall addition step (R4 + R5) is exothermic and therefore likely to proceed in the gas phase. More recent experiments and computations indicate that the empirically formulated HgO_2 is the linear OHgO molecule that is ∼167 kJ mol^{-1} (in the $^3\sum_g^-$ state) more stable than $Hg(^3P)$ + O_2.[41] In addition to exothermic dissociation to $Hg(^1S)$ and O_2 feasible via the asymmetric

https://doi.org/10.1021/acs.est.2c02722
Environ. Sci. Technol. 2022, 56, 13428−13438

HgOO isomer, OHgO can react further to HgO by O transfer to either dioxygen or to its odd oxygen analogues (O_3 and O atoms) (Figure 6). R7 is approximately of the same magnitude as the activation energy of the oxidation, while the reactions with odd oxygen are clearly exoergic. However, there are doubts about the stability of the proposed product HgO, which as a molecule is only slightly more stable (~21 kJ mol^{-1}) than $Hg(^1S) + O(^3P)$.[42] Recent high-level ab initio calculations predict a triplet ($^3\Pi$) ground state for HgO prone to oligomerization.[43] The dissociation energy of 222 ± 33 kJ mol^{-1} determined by Grade and Hirschwald[44] possibly corresponds to an oligomer rather than a single HgO molecule.[43] This argument has been supported experimentally by laser desorption ionization time-of-flight mass spectrometry (LDI-TOF MS) on solid HgO,[45] which shows that the HgO molecule is marginally stable in the gas phase and promptly polymerizes into $(HgO)_n$ clusters (instrumentation upper detection limit $n \leq 34$) or dissociates when exposed to light (355 nm). The photopolymerization may be written as

$$2HgO \rightleftarrows (HgO)_2 \xleftrightarrow{n\text{HgO}} (HgO)_{2+n} \xrightarrow{n\geq 4} \xrightarrow{\text{polymerization}} HgO(s) \quad \text{(R8)}$$

where dissociation for $\geq 2 + n = 6$ oligomers was not detected in LDI-TOF MS spectra.[45] Photo- and thermal decomposition of molecular HgO follow[46]

$$HgO \xrightarrow{h\nu/M} Hg(^1S) + O(^3P) \quad \text{(R9)}$$

The absorption spectrum of HgO(g) ($\lambda > 254$ nm) exhibits a shape that is essentially structureless, which concludes that R9 proceeds via a direct photodissociation mechanism. A limitation in the gas-phase chain formation en route, via aggregation, to solid HgO[41] (R8) is the lifetime of the initiating molecule HgO.[46] Net formation of HgO(s) occurs in laboratory studies,[17,19] but it cannot be ruled out that this is due to control by wall reactions inside the reactor and therefore photosynthesis of HgO in the atmosphere may be viewed with skepticism.[18] Although Hg gas-phase oxidation in, e.g., polar air has been attributed as a source of new particle formation,[47] polymerization can be dismissed as a viable pathway for stabilizing the product in the atmosphere, reactions with major species that can convert HgO to a fully two-coordinated Hg binding environment are strongly favored. Unlike solid and aqueous phases where the species is not known, $Hg(OH)_2$ has been identified as a very stable molecule in the gas phase against photolysis[41,48] and the reaction between HgO and water vapor is enormously favorable with the product of about 238 kJ mol^{-1} lower in energy[49]

$$HgO(g) + H_2O(g) \rightarrow Hg(OH)_2(g) \quad \text{(R10)}$$

As with O_2, Hg can photosensitize the H_2O molecule, and experiments with $Hg(^3P) + H_2O$ gas mixtures give rise to net oxidation of Hg vapor.[40] Although R10 and analogous reactions with the smallest oligomers of HgO (Figure 6) may theoretically be attributed to mitigate for the high probability of prompt dissociation (R9), they are however hitherto experimentally uncharacterized, extremely challenging to examine, and are beyond the scope of this study.

Given that MIF detection is limited to elements with at least three stable isotopes, substantial dissociative MIF in the photolysis of molecular gases is common for those bearing oxygen (three stable isotopes) and/or sulfur (four stable isotopes).[50] The intricacies of dissociation are complex to model, particularly when the system of interest is at the isotopic level. Several theoretical attempts have been made to understand dissociative MIF in the gaseous phase qualitatively, as a diatomic direct dissociative process such as R9 excludes self-shielding and symmetry dependence as the mechanism but not kinetic MIF-effects associated with, e.g., different state-to-state transition probabilities of the isotopomers from a bound state ultimately to dissociated products.[51] New findings on atmospheric Hg chemistry have supported that photodissociation mechanisms are fundamentally important and cause major molecular Hg^{II} species to revert rapidly directly to Hg or indirectly via Hg^{I} radicals.[1] The reaction steps considered for dissociative MIF are R9 and the hypothetical HgOO → $Hg(^1S) + O_2$ (Figure 6), while the actions of isotope exchange reactions and other mass-dependent processes gradually remove the imprinted MIF unless the effect is captured in a stable product. In addition to photodissociation of monomers, photopolymerization accompanied with MIF has been experimentally confirmed[50] and theoretically discussed.[52] Harman et al.[52] argue that the back reactions for certain oligomers during the chain formation trigger MIF, which here relates to the decomposition of the smallest HgO clusters (especially the dimer) in R8. These clusters are considerably less stabilized relative to the parent HgO molecule than the case for larger clusters ($2 + n \geq 6$), which are more strongly bound by an energy approaching that for one-dimensional crystalline HgO (−268.4 kJ mol^{-1}).[49] From LDI-TOF MS spectra, it appears that the photodecomposition of $(HgO)_{2+n<6}$ proceeds not only by fragmentation into smaller HgO units but also by the formation of clusters with Hg−Hg bonds after oxygen atoms have been abstracted.[45]

In summary, the net oxidation in the UVC-irradiated Hg−O_2 system follows a pressure- and temperature-dependent kinetics corresponding to a chemically activated gas-phase reaction (R4−R6). Further details of the reaction mechanism are obtained from the observation that MIF increases under higher pressure and temperature (Figures 4 and 5), which is compatible with the decomposition of HgO_x species (e.g., R9 and R4) being thermally conditioned and affected by a third body (M). Atmospheric photodissociation as the origin of anomalous fractionation of both odd (^{33}S) and even (^{36}S) isotopes was observed for S without, despite considerable effort, knowing clearly through which underlying processes. The emergence of anomalous Hg isotope fractionation can be traced to the marginal stability of HgO_x and the smallest HgO oligomers with respect to fragmentation. We have also demonstrated diminishing fractionation factors with the increasing net oxidation rate, which has been attributed to the occurrence of a multiple-step reaction.[53] The reaction scheme applicable to the laboratory experiments is summarized in Figure 6. As aforementioned, oligomerization cannot be attributed to any significance in the atmosphere and the potential role of water vapor as a reactant in secondary chemistry leading to stable mercuric hydroxide compounds with imprinted MIF has been indicated in the figure.

Implications of Atmospheric Sources of even-Hg-MIF. The substantial span in $\delta^{xxx}Hg$ observations under the experimental conditions of this work is largely an effect of the pressure and temperature dependence of the multistep reversible processes of HgO_x outlined above inducing MIF, which in turn influences the magnitudes of odd- and even-MIF signatures as well as the diagnostic ratios of $\Delta^{200}Hg$ to $\Delta^{204}Hg$

https://doi.org/10.1021/acs.est.2c02722
Environ. Sci. Technol. 2022, 56, 13428−13438

and Δ^{199}Hg to Δ^{201}Hg. The regulation of the atmospheric odd-MIF has been thought to be controlled through aerosol photoreduction (−MIE) and photoreduction in surface reservoirs that give rise to Hg effluxes into the atmosphere (e.g., plant- and snow-sourced: +MIE,[54] soil- and marine-sourced: −MIE[55]), while anthropogenic Hg input to the atmosphere carries near-zero Δ^{199}Hg and Δ^{201}Hg.[29] The mass flow through the above-mentioned photochemical channels is large[56] compared to that of gaseous HgO photoreduction. The latter is of minor relevance in determining the odd-MIF of atmospheric Hg and was evidenced by the large even-MIF triggered by photofragmentation. The process results in negative Δ^{200}Hg in unreacted Hg and positive Δ^{200}Hg in the product following Δ^{200}Hg/Δ^{204}Hg ratios that for free tropospheric temperature and pressure conditions investigated are similar to those observed in global precipitation samples.

When assessing the possibility of an Arctic even-MIF source, Mead et al.[8] concluded that the slant column densities of atmospheric Hg (~10^{18} atoms m^{-2} assuming a Hg concentration of 1.5 ng m^{-3}) that solar irradiance passes during winter at high latitudes exceed the perpendicular ones at the tropics by one order of magnitude. However, due to the stratospheric O_3 layer, actinic sunlight lacking UVC (especially lacking ~185 and ~254 nm bands) may preclude tropospheric photoproduction of Hg(^{3}P) atoms. Above 30 km, R4 operates by the abundance of UVC radiation generating Hg(^{3}P) and Hg(^{1}P) atoms.[16,25] There is emerging evidence that significant concentrations of stratospheric Hg exist only up to 4 km above the tropopause.[57] Extrapolation of our measurement data to stratospheric pressure levels (only small even-MIF triggered, Table S4) in combination with very low Hg concentrations indicates that these reactions as a stratospheric source of even-MIF are not likely.

There are major gas-phase reactions in the lower atmosphere that can lead to photochemical production of HgO as a MIF source by subsequent dissociation. Gross atmospheric Hg oxidation is initiated by Br atoms[58] and plausibly also by OH radicals,[48,59] which follow analogous two-step processes (hereinafter for the Br case)

$$Hg(^1S) + Br + M \rightleftarrows BrHg^I + M \quad (R11)$$

$$BrHg^I + Y \xrightarrow{M} BrHg^{II}Y \quad (R12)$$

where Y is an abundant radical. In a previous study, we examined R11 and R12 (Y = Br) at room temperature without finding definite evidence of significant even-MIF.[11] Recent computational studies[46,60] suggest that atmospheric products from R12, $BrHg^{II}OOH$, and *syn*-$BrHg^{II}ONO$ readily photodissociate in the atmosphere yielding $BrHg^{II}O$, which alternatively can be produced by oxidation of $BrHg^I$ by ozone[1]. Analogously, $HOHg^{II}O$ can be formed by the $HOHg^I$ + O_3 reaction.[48] As for $BrHg^{II}OOH$ and *syn*-$BrHg^{II}ONO$, no experimental data exist for $BrHg^{II}O$ and $HOHg^{II}O$. However, theoretical calculations suggest that these oxides are photolabile yet stable with respect to thermal dissociation with a stronger Hg−O bond than in molecular $Hg^{II}O$.[61] The atmospheric fate of the proposed key intermediates $ZHg^{II}O$ (Z = Br and OH) is governed by photodissociation,[46] abstraction of a H atom from CH_4,[60] and reduction by CO.[62] Photolysis of $ZHg^{II}O$ (atmospheric lifetime ~ 30 s for $BrHg^{II}O$) takes place by breaking the Hg−Z bond with HgO as the primary photoproduct[46]

$$ZHg^{II}O \xrightarrow{h\nu} Hg^{II}O + Z \quad (R13)$$

Thus, if R13 has atmospheric significance, it is doubtful whether gas-phase Hg(^{3}P)-initiated processes and other potential Hg(^{1}S) oxidation schemes[18] can photosynthesize HgO. Nevertheless, a state-of-the-art global model with comprehensive Hg, Hg^I, and Hg^{II} chemistry (CAM-Chem) evaluated against atmospheric Hg observations infers missing Hg oxidation pathways in the lower atmosphere (e.g., simulated wet deposition is underestimated).[1] Although these pathways remain to be identified,[48] it is required that the product is considerably more stable than those from R13 for the oxidation step to be significant with respect to photoreduction or that Hg^{II} species formed are rapidly stabilized (R10). Precipitations carrying the largest observed even-MIF signatures[6] and increased Hg^{II} wet deposition have been linked to convective precipitation[63] and thunderstorms.[64] Kaulfus et al.[65] found that the highest Hg^{II} deposition is caused by high-reaching supercell thunderstorms characterized by an excessive amount of lightning. Precipitation data from the tropics show a strong positive correlation between wet Hg^{II} concentration and the maximum height in cloud where rain is detected (echo tops).[63] Evidence exists for formation of Hg^{II} at higher altitudes in the tropopause region[66] and several km up in the stratosphere is generally aerosol-bound Hg^{II} detected with a relatively high Hg content in small particles at nanometer size.[67] Unlike stratospheric Hg^{II}, significant losses of Hg^{II} below the tropopause occur through convective cloud scavenging.[66]

If phase equilibrium is assumed for Hg^{II}, a parameterization based on temperature and PM2.5[31] gives that >99% Hg^{II} is attached to particles at a conservatively low tropopause aerosol level.[68] In addition, the temperature of down to −50 °C stabilizes intermediates that promote net oxidation.[60] A compilation of measured Hg^{II} altitude profiles shows a global maximum at 15 km altitude (~0.25 ng m^{-3}), which CAM-Chem simulations with the updated $Hg^{I,II}$ photochemistry severely underestimated.[1] According to Francés-Monerris et al.,[46] R13, the main source of tropospheric HgO, occurs at a rate of 0.56 × J(BrHgO), where J(BrHgO) is 2.95 × 10^{-2} s^{-1} in the global troposphere. For photoproduction of HgO via R7 in the upper troposphere, approximated from J (253 K, 45 kPa) estimated in this work and of the same magnitude as that from R13 under actinic light, a photon flux of ~2 × 10^{13} cm^{-2} s^{-1} at 253.7 nm is required. Although it cannot be ruled out that discrete photon fluxes of similar magnitude may be produced in the blackbody radiation from powerful cloud-to-ground lightnings (>10,000 K),[69] it is unrealistic to attribute any global significance to Hg(^{3}P)-induced oxidation, in addition to the low solar UVC flux in the upper stratosphere.[16] The similarities in Δ^{200}Hg/Δ^{204}Hg observations between the laboratory experiments and atmospheric samples point to a possible chemical process that labile molecules such as HgO are bearing intermediates in the atmospheric redox chemistry of mercury. The emergence of even-MIF in the absence of plausible oxidation channels requires further theoretical and experimental investigations. Excluding LDI-TOF MS experiments with solid HgO as the source,[45] gaseous HgO lacks experimental characterization. Assessment of the stability and potential reactions of HgO (R10) requires advanced laser spectroscopic methods, which possibly generate robust levels of HgO through the spin-allowed and thus fast Hg(^{1}S) + O(^{1}D) reaction. In addition to laboratory studies, future field

https://doi.org/10.1021/acs.est.2c02722
Environ. Sci. Technol. 2022, 56, 13428−13438

experiments reporting isotopic Hg and Hg^{II} vertical profiles in the atmosphere may help further constrain even-MIF sources.

■ ASSOCIATED CONTENT

Supporting Information

The Supporting Information is available free of charge at https://pubs.acs.org/doi/10.1021/acs.est.2c02722.

Complementary materials including details of the reaction mechanism, Figures related to, e.g., experimental setup, photolytical source, and isotope fractionation details, and Tables showing, e.g., experimental conditions, QA/QC, kinetics, and comprehensive isotopic sample data (PDF)

■ AUTHOR INFORMATION

Corresponding Authors

Xinbin Feng − *State Key Laboratory of Environmental Geochemistry, Institute of Geochemistry, Chinese Academy of Sciences, Guiyang 550081, China; Center for Excellence in Quaternary Science and Global Change, Chinese Academy of Sciences, Xian 710061, China;* orcid.org/0000-0002-7462-8998; Phone: +86-851-85895728; Email: fengxinbin@vip.skleg.cn; Fax: +86-851-85891721

Jonas Olof Sommar − *State Key Laboratory of Environmental Geochemistry, Institute of Geochemistry, Chinese Academy of Sciences, Guiyang 550081, China;* orcid.org/0000-0001-8634-440X; Phone: +86-018275032610; Email: jonas@vip.skleg.cn; Fax: +86-851-85891721

Authors

Guangyi Sun − *State Key Laboratory of Environmental Geochemistry, Institute of Geochemistry, Chinese Academy of Sciences, Guiyang 550081, China;* orcid.org/0000-0001-8522-7973

Runsheng Yin − *State Key Laboratory of Ore Deposit Geochemistry, Institute of Geochemistry, Chinese Academy of Sciences, Guiyang 550081, China*

Feiyue Wang − *Centre for Earth Observation Science, and Department of Environment and Geography, University of Manitoba, Winnipeg, Manitoba R3T 2N2, Canada;* orcid.org/0000-0001-5297-0859

Che-Jen Lin − *State Key Laboratory of Environmental Geochemistry, Institute of Geochemistry, Chinese Academy of Sciences, Guiyang 550081, China; Center for Advances in Water and Air Quality, Lamar University, Beaumont, Texas 777100, United States*

Kai Li − *State Key Laboratory of Environmental Geochemistry, Institute of Geochemistry, Chinese Academy of Sciences, Guiyang 550081, China; University of Chinese Academy of Sciences, Beijing 100045, China*

Complete contact information is available at: https://pubs.acs.org/10.1021/acs.est.2c02722

Author Contributions

G.S., J.S., and X.F. designed research, G.S., X.F., R.Y., F.W., C.-J.L., K.L., and J.S. performed research, G.S., J.S., and X.F. analyzed data, J.S. and G.S. wrote the manuscript, and all coauthors contributed to the interpretation of the results and to the text. All authors read the manuscript and approved the submission.

Notes

The authors declare no competing financial interest.

All data generated or analyzed during this study are included in this published article and its supplement. The original Hg isotopic results from the experiments are given in Tables S4 and S5.

■ ACKNOWLEDGMENTS

This work was jointly supported by the National Natural Science Foundation of China (41773146, 41907286, and 41921004), the Key Research Program of Frontier Science of the Chinese Academy of Sciences (QYZDJ-SSW-DQC005), and the China Postdoctoral Science Foundation [grant numbers 2018M640939 and 2020T130649]. The authors are grateful to Caihong Gao and Yun Liu of IGCAS for helpful discussions in theoretical isotope geochemistry.

■ REFERENCES

(1) Saiz-Lopez, A.; Travnikov, O.; Sonke, J. E.; Thackray, C. P.; Jacob, D. J.; Carmona-Garcia, J.; Frances-Monerris, A.; Roca-Sanjuan, D.; Acuna, A. U.; Davalos, J. Z.; Cuevas, C. A.; Jiskra, M.; Wang, F.; Bieser, J.; Plane, J. M. C.; Francisco, J. S. Photochemistry of oxidized Hg(I) and Hg(II) species suggests missing mercury oxidation in the troposphere. *Proc. Natl. Acad. Sci. U.S.A.* **2020**, *117*, 30949−30956.

(2) Motta, L. C.; Chien, A. D.; Rask, A. E.; Zimmerman, P. M. Mercury Magnetic Isotope Effect: A Plausible Photochemical Mechanism. *J. Phys. Chem. A* **2020**, *124*, 3711−3719.

(3) Schauble, E. A. Role of nuclear volume in driving equilibrium stable isotope fractionation of mercury, thallium, and other very heavy elements. *Geochim. Cosmochim. Acta* **2007**, *71*, 2170−2189.

(4) Gratz, L. E.; Keeler, G. J.; Blum, J. D.; Sherman, L. S. Isotopic Composition and Fractionation of Mercury in Great Lakes Precipitation and Ambient Air. *Environ. Sci. Technol.* **2010**, *44*, 7764−7770.

(5) Kwon, S. Y.; Blum, J. D.; Yin, R.; Tsui, M. T.-K.; Yang, Y. H.; Choi, J. W. Mercury stable isotopes for monitoring the effectiveness of the Minamata Convention on Mercury. *Earth-Sci. Rev.* **2020**, *203*, No. 103111.

(6) Fu, X.; Jiskra, M.; Yang, X.; Marusczak, N.; Enrico, M.; Chmeleff, J.; Heimbürger-Boavida, L.-E.; Gheusi, F.; Sonke, J. E. Mass-Independent Fractionation of Even and Odd Mercury Isotopes during Atmospheric Mercury Redox Reactions. *Environ. Sci. Technol.* **2021**, *55*, 10164−10174.

(7) Chen, J.; Hintelmann, H.; Feng, X.; Dimock, B. Unusual fractionation of both odd and even mercury isotopes in precipitation from Peterborough, ON, Canada. *Geochim. Cosmochim. Acta* **2012**, *90*, 3346.

(8) Mead, C.; Lyons, J. R.; Johnson, T. M.; Anbar, A. D. Unique Hg Stable Isotope Signatures of Compact Fluorescent Lamp-Sourced Hg. *Environ. Sci. Technol.* **2013**, *47*, 2542−2547.

(9) Blum, J. D.; Johnson, M. W. Recent developments in mercury stable isotope analysis. *Rev. Mineral. Geochem.* **2017**, *82*, 733−757.

(10) Zerkle, A. L.; Yin, R.; Chen, C.; Li, X.; Izon, G. J.; Grasby, S. E. Anomalous fractionation of mercury isotopes in the Late Archean atmosphere. *Nat. Commun.* **2020**, *11*, No. 1709. Meixnerová, J.; Blum, J. D.; Johnson, M. W.; Stüeken, E. E.; Kipp, M. A.; Anbar, A. D.; Buick, R. Mercury abundance and isotopic composition indicate subaerial volcanism prior to the end-Archean"whiff" of oxygen. *Proc. Natl. Acad. Sci. U.S.A.* **2021**, *118*, No. e2107511118.

(11) Sun, G.; Sommar, J.; Feng, X.; Lin, C.-J.; Ge, M.; Wang, W.; Yin, R.; Fu, X.; Shang, L. Mass -dependent and -independent fractionation of mercury isotope during gas-phase oxidation of elemental mercury vapor by atomic Cl and Br. *Environ. Sci. Technol.* **2016**, *50*, 9232−9241.

(12) Wang, X.; Jacob, D. J.; Downs, W.; Zhai, S.; Zhu, L.; Shah, V.; Holmes, C. D.; Sherwen, T.; Alexander, B.; Evans, M. J.; Eastham, S. D.; Andrew Neuman, J.; Veres, P.; Koenig, T.; Vollamer, R.; Gregory Huey, L.; Bannan, T.; Percival, C.; Lee, B.; Thornton, J. Global

tropospheric halogen (Cl, Br, I) chemistry and its impact on oxidants. *Atmos. Chem. Phys.* **2021**, *21*, 13973−13996.
(13) Hall, B.; Schager, P.; Weesmaa, J. The Homogeneous Gas-Phase Reaction of Mercury with Oxygen, and the Corresponding Heterogeneous Reactions in the Presence of Activated Carbon and Fly-Ash. *Chemosphere* **1995**, *30*, 611−627.
(14) Callear, A. B.; McGurk, J. C. Flash Spectroscopy with Mercury Resonance Radiation. 5. Formation and Relaxation of $Hg(6^3P_0)$. *J. Chem. Soc., Faraday Trans. 2* **1973**, *69*, 97−114.
(15) Hippler, H.; Wendt, H. R.; Hunziker, H. E. Excited intermediates in Hg-photosensitized reaction of O_2 detected by energy-transfer. *J. Chem. Phys.* **1978**, *68*, 5103−5111.
(16) Finlayson-Pitts, B. J.; Pitts, J. N. *Chemistry of the Upper and Lower Atmosphere: Theory, Experiments and Applications*; Academic Press, 2000, pp 1−969.
(17) Dickinson, R. G.; Sherrill, M. S. Formation of Ozone by Optically Excited Mercury Vapor. *Proc. Natl. Acad. Sci. U.S.A.* **1926**, *12*, 175−178.
(18) Hynes, A. J.; Donohoue, D. L.; Goodsite, M. E.; Hedgecock, I. M. Our Current Understanding of Major Chemical and Physical Processes Affecting Mercury Dynamics in the Atmosphere and at the Air-Water/Terrestrial Interfaces. In *Mercury Fate and Transport in the Global Atmosphere - Emissions, Measurements and Models*; Mason, R. P.; Pirrone, N. Eds.; Springer, 2009; pp 427−457.
(19) Callear, A. B.; Patrick, C. R.; Robb, J. C. Reaction of excited mercury (Hg 6^3P_1) with oxygen. *Trans. Faraday Soc.* **1959**, *55*, 280−287.
(20) Vyazovetskii, Y. V. Photochemical production of the ^{204}Hg isotope. *Tech. Phys.* **2012**, *57*, 603−607.
(21) Sholupov, S.; Pogarev, S.; Ryzhov, V.; Mashyanov, N.; Stroganov, A. Zeeman atomic absorption spectrometer RA-915+for direct determination of mercury in air and complex matrix samples. *Fuel Process. Technol.* **2004**, *85*, 473−485.
(22) Bergquist, B. A.; Blum, J. D. Mass-dependent and -independent fractionation of Hg isotopes by photoreduction in aquatic systems. *Science* **2007**, *318*, 417−420.
(23) Mei, L.; Zhao, G.; Svanberg, S. Differential absorption lidar system employed for background atomic mercury vertical profiling in South China. *Opt. Lasers Eng.* **2014**, *55*, 128−135.
(24) Carstensen, H.-H.; Dean, A. M. The Kinetics of Pressure-Dependent Reactions. In *Comprehensive Chemical Kinetics*, Carr, R. W., Ed.; Elsevier, 2007; Chapter 4, Vol. *42*, pp 101−184.
(25) Okabe, H. *Photochemistry of Small Molecules*; Wiley-Interscience, 1978.
(26) Volman, D. H. The Photochemical Formation of Ozone. Foreign Gas Effects on the Mercury Sensitized Reaction at 2537 Å and the Unsensitized Reaction at 1849 Å. *J. Am. Chem. Soc.* **1954**, *76*, 6034−6036.
(27) Young, E. D.; Galy, A.; Nagahara, H. Kinetic and equilibrium mass-dependent isotope fractionation laws in nature and their geochemical and cosmochemical significance. *Geochim. Cosmochim. Acta* **2002**, *66*, 1095−1104.
(28) Cai, H.; Chen, J. Mass-independent fractionation of even mercury isotopes. *Sci. Bull.* **2015**, 1−9.
(29) Sommar, J.; Osterwalder, S.; Zhu, W. Recent advances in understanding and measurement of Hg in the environment: Surface-atmosphere exchange of gaseous elemental mercury (Hg^0). *Sci. Total Environ.* **2020**, *721*, No. 137648.
(30) Holmes, C. D.; Jacob, D. J.; Corbitt, E. S.; Mao, J.; Yang, X.; Talbot, R.; Slemr, F. Global atmospheric model for mercury including oxidation by bromine atoms. *Atmos. Chem. Phys.* **2010**, *10*, 12037−12057.
(31) Amos, H. M.; Jacob, D. J.; Holmes, C. D.; Fisher, J. A.; Wang, Q.; Yantosca, R. M.; Corbitt, E. S.; Galarneau, E.; Rutter, A. P.; Gustin, M. S.; Steffen, A.; Schauer, J. J.; Graydon, J. A.; Louis, V.; Talbot, R.; Edgerton, E. S.; Zhang, Y.; Sunderland, E. M. Gas-particle partitioning of atmospheric Hg(II) and its effect on global mercury deposition. *Atmos. Chem. Phys.* **2012**, *12*, 591−603.
(32) Steiner, U. E.; Ulrich, T. Magnetic field effects in chemical kinetics and related phenomena. *Chem. Rev.* **1989**, *89*, 51−147.
(33) Motta, L. C.; Kritee, K.; Blum, J. D.; Tsz-Ki Tsui, M.; Reinfelder, J. R. Mercury Isotope Fractionation during the Photochemical Reduction of Hg(II) Coordinated with Organic Ligands. *J. Phys. Chem. A* **2020**, *124*, 2842−2853.
(34) Yang, S.; Liu, Y. Nuclear volume effects in equilibrium stable isotope fractionations of mercury, thallium and lead. *Sci. Rep.* **2015**, *5*, No. 12626.
(35) Mulder, B. J.; Vanheusden, S. Mechanism of glass darkening by a low-pressure mercury discharge. *J. Electrochem. Soc.* **1983**, *130*, 440−449.
(36) Thiemens, M. H. History and applications of mass-independent isotope effects. *Annu. Rev. Earth Planet. Sci.* **2006**, *34*, 217−262.
(37) Lawler, J. E.; Raizen, M. G. Enhanced escape rate for Hg 254 nm resonance radiation in fluorescent lamps. *J. Phys. D: Appl. Phys.* **2013**, *46*, No. 415204.
(38) Sommerer, T. J. A Monte Carlo simulation of resonance radiation transport in the rare-gas−mercury positive column. *J. Appl. Phys.* **1993**, *74*, 1579−1589.
(39) Halstead, J. A.; Reeves, R. R. Determination of the lifetime of the mercury 6^3P_1 state. *J. Quant. Spectrosc. Radiat. Transfer* **1982**, *28*, 289−296.
(40) Desnoyer, M.; Nief, G.; Roth, E. Oxydation photochimique du mercure et sélectivité isotopique. *J. Chim. Phys.* **1963**, *60*, 209−211.
(41) Wang, X. F.; Andrews, L. Infrared spectrum of $Hg(OH)_2$ in solid neon and argon. *Inorg. Chem.* **2005**, *44*, 108−113.
(42) Peterson, K. A.; Shepler, B. C.; Singleton, J. M. The group 12 metal chalcogenides: an accurate multireference configuration interaction and coupled cluster study. *Mol. Phys.* **2007**, *105*, 1139−1155.
(43) Cremer, D.; Kraka, E.; Filatov, M. Bonding in Mercury Molecules Described by the Normalized Elimination of the Small Component and Coupled Cluster Theory. *ChemPhysChem* **2008**, *9*, 2510−2521.
(44) Grade, M.; Hirschwald, W. Energetics and stabilities of the IIB/VIA-compounds at high-temperature equilibrium conditions. *Ber. Bunsen-Ges.* **1982**, *86*, 899−907.
(45) Jayasekharan, T.; Sahoo, N. K. Mercury mono oxide cluster ions $(HgO)_n^+$ by laser desorption ionization time of flight mass spectrometry. *J. Mass Spectrom.* **2014**, *49*, 248−250.
(46) Francés-Monerris, A.; Carmona-García, J.; Acuña, A. U.; Dávalos, J. Z.; Cuevas, C. A.; Kinnison, D. E.; Francisco, J. S.; Saiz-Lopez, A.; Roca-Sanjuán, D. Photodissociation Mechanisms of Major Mercury(II) Species in the Atmospheric Chemical Cycle of Mercury. *Angew. Chem., Int. Ed.* **2020**, *59*, 7605−7610.
(47) Humphries, R. S.; Schofield, R.; Keywood, M. D.; Ward, J.; Pierce, J. R.; Gionfriddo, C. M.; Tate, M. T.; Krabbenhoft, D. P.; Galbally, I. E.; Molloy, S. B.; Klekociuk, A. R.; Johnston, P. V.; Kreher, K.; Thomas, A. J.; Robinson, A. D.; Harris, N.; Johnson, R.; Wilson, S. R. Boundary layer new particle formation over East Antarctic sea ice − possible Hg-driven nucleation? *Atmos. Chem. Phys.* **2015**, *15*, 13339−13364.
(48) Shah, V.; Jacob, D.; Thackray, C.; Wang, X.; Sunderland, E.; Dibble, T.; Saiz-Lopez, A.; Cernusak, I.; Kellö, V.; Castro, P.; Wu, R.; Wang, C. Improved Mechanistic Model of the Atmospheric Redox Chemistry of Mercury. *Environ. Sci. Technol.* **2021**, *55*, 14445−14456.
(49) Tossell, J. A. Calculation of the energetics for the oligomerization of gas phase HgO and HgS and for the solvolysis of crystalline HgO and HgS. *J. Phys. Chem. A* **2006**, *110*, 2571−2578.
(50) Colman, J. J.; Xu, X.; Thiemens, M. H.; Trogler, W. C. Photopolymerization and Mass-Independent Sulfur Isotope Fractionations in Carbon Disulfide. *Science* **1996**, *273*, 774−776.
(51) Thiemens, M. H.; Lin, M. Discoveries of Mass Independent Isotope Effects in the Solar System: Past, Present and Future. *Rev. Mineral. Geochem.* **2021**, *86*, 35−95. Masterson, A. L.; Farquhar, J.; Wing, B. A. Sulfur mass-independent fractionation patterns in the broadband UV photolysis of sulfur dioxide: Pressure and third body effects. *Earth Planet. Sci. Lett.* **2011**, *306*, 253−260.

https://doi.org/10.1021/acs.est.2c02722
Environ. Sci. Technol. 2022, 56, 13428−13438

(52) Harman, C. E.; Pavlov, A. A.; Babikov, D.; Kasting, J. F. Chain formation as a mechanism for mass-independent fractionation of sulfur isotopes in the Archean atmosphere. *Earth Planet. Sci. Lett.* **2018**, *496*, 238−247.
(53) Vieten, B.; Blunier, T.; Neftel, A.; Alewell, C.; Conen, F. Fractionation factors for stable isotopes of N and O during N_2O reduction in soil depend on reaction rate constant. *Rapid Commun. Mass Spectrom.* **2007**, *21*, 846−850.
(54) Yuan, W.; Sommar, J.; Lin, C.-J.; Wang, X.; Li, K.; Liu, Y.; Zhang, H.; Lu, Z.; Wu, C.; Feng, X. Stable Isotope Evidence Shows Re-emission of Elemental Mercury Vapor Occurring after Reductive Loss from Foliage. *Environ. Sci. Technol.* **2019**, *53*, 651−660. Kurz, A. Y.; Blum, J.; Johnson, M.; Nadelhoffer, K.; Zak, D. Isotopic composition of mercury deposited via snow into mid-latitude ecosystems. *Sci. Total Environ.* **2021**, *784*, No. 147252.
(55) Zhang, H.; Tan, Q.; Zhang, L.; Fu, X.; Feng, X. A Laboratory Study on the Isotopic Composition of Hg(0) Emitted From Hg-Enriched Soils in Wanshan Hg Mining Area. *J. Geophys. Res.: Atmos.* **2020**, *125*, No. e2020JD032572.
(56) Sun, R. Y.; Jiskra, M.; Amos, H. M.; Zhang, Y. X.; Sunderland, E. M.; Sonke, J. E. Modelling the mercury stable isotope distribution of Earth surface reservoirs: Implications for global Hg cycling. *Geochim. Cosmochim. Acta* **2019**, *246*, 156−173.
(57) Slemr, F.; Weigelt, A.; Ebinghaus, R.; Bieser, J.; Brenninkmeijer, C. A. M.; Rauthe-Schoch, A.; Hermann, M.; Martinsson, B. G.; van Velthoven, P.; Bonisch, H.; Neumaier, M.; Zahn, A.; Ziereis, H. Mercury distribution in the upper troposphere and lowermost stratosphere according to measurements by the IAGOS-CARIBIC observatory: 2014-2016. *Atmos. Chem. Phys.* **2018**, *18*, 12329−12343.
(58) Donohoue, D. L.; Bauer, D.; Cossairt, B.; Hynes, A. J. Temperature and Pressure Dependent Rate Coefficients for the Reaction of Hg with Br and the Reaction of Br with Br: A Pulsed Laser Photolysis-Pulsed Laser Induced Fluorescence Study. *J. Phys. Chem. A* **2006**, *110*, 6623−6632.
(59) Sommar, J.; Gårdfeldt, K.; Strömberg, D.; Feng, X. B. A kinetic study of the gas-phase reaction between the hydroxyl radical and atomic mercury. *Atmos. Environ.* **2001**, *35*, 3049−3054. Dibble, T. S.; Tetu, H. L.; Jiao, Y. G.; Thackray, C. P.; Jacob, D. J. Modeling the OH-Initiated Oxidation of Mercury in the Global Atmosphere without Violating Physical Laws. *J. Phys. Chem. A* **2020**, *124*, 444−453.
(60) Lam, K. T.; Wilhelmsen, C. J.; Schwid, A. C.; Jiao, Y.; Dibble, T. S. Computational Study on the Photolysis of BrHgONO and the Reactions of $BrHgO^{\bullet}$ with CH_4, C_2H_6, NO, and NO_2: Implications for Formation of Hg(II) Compounds in the Atmosphere. *J. Phys. Chem. A* **2019**, *123*, 1637−1647.
(61) Balabanov, N. B.; Peterson, K. A. Accurate theoretical near-equilibrium potential energy and dipole moment surfaces of HgClO and HgBrO. *J. Chem. Phys.* **2004**, *120*, 6585−6592.
(62) Khiri, D.; Louis, F.; Cernusak, I.; Dibble, T. S. $BrHgO\cdot$ + CO: Analogue of OH plus CO and Reduction Path for Hg(II) in the Atmosphere. *ACS Earth Space Chem.* **2020**, *4*, 1777−1784.
(63) Shanley, J. B.; Engle, M. A.; Scholl, M.; Krabbenhoft, D. P.; Brunette, R.; Olson, M. L.; Conroy, M. E. High Mercury Wet Deposition at a "Clean Air" Site in Puerto Rico. *Environ. Sci. Technol.* **2015**, *49*, 12474−12482.
(64) Holmes, C. D.; Krishnamurthy, N. P.; Caffrey, J. M.; Landing, W. M.; Edgerton, E. S.; Knapp, K. R.; Nair, U. S. Thunderstorms Increase Mercury Wet Deposition. *Environ. Sci. Technol.* **2016**, *50*, 9343−9350.
(65) Kaulfus, A. S.; Nair, U.; Holmes, C. D.; Landing, W. M. Mercury Wet Scavenging and Deposition Differences by Precipitation Type. *Environ. Sci. Technol.* **2017**, *51*, 2628−2634.
(66) Lyman, S. N.; Jaffe, D. Formation and fate of oxidized mercury in the upper troposphere and lower stratosphere. *Nat. Geosci.* **2012**, *5*, 114−117.
(67) Murphy, D. M.; Hudson, P. K.; Thomson, D. S.; Sheridan, P. J.; Wilson, J. C. Observations of mercury-containing aerosols. *Environ. Sci. Technol.* **2006**, *40*, 3163−3167.
(68) Martinsson, B. G.; Friberg, J.; Andersson, S. M.; Weigelt, A.; Hermann, M.; Assmann, D.; Voigtländer, J.; Brenninkmeijer, C. A. M.; van Velthoven, P. J. F.; Zahn, A. Comparison between CARIBIC Aerosol Samples Analysed by Accelerator-Based Methods and Optical Particle Counter Measurements. *Atmos. Meas. Tech.* **2014**, *7*, 2581−2596.
(69) Orville, R. E.; Henderson, R. W. Absolute Spectral Irradiance Measurements of Lightning from 375 to 880 nm. *J. Atmos. Sci.* **1984**, *41*, 3180−3187.

NOTE ADDED AFTER ASAP PUBLICATION

This paper was published ASAP on August 12, 2022 with errors in the text. The corrected version was reposted on August 23, 2022.

https://doi.org/10.1021/acs.est.2c02722
Environ. Sci. Technol. 2022, 56, 13428−13438